PCCP

Accepted Manuscript

ROYAL SOCIETY OF CHEMISTRY

www.rsc.org/pccp

Journal Name

ARTICLE TYPE

Cite this: DOI: 10.1039/xxxxxxxxxx

Self-assembly of block copolymers on lithographically patterned template with ordered posts†

Dan Xu,[a] Hong Liu,*[a,b‡], Yao-Hong Xue[c] and Yan-Bo Sun[d]

Received Date
Accepted Date

DOI: 10.1039/xxxxxxxxxx

www.rsc.org/journalname

The dissipative particle dynamics simulations are employed to study the self-assembly of block copolymers on the template modified with ordered posts. The templates with hexagonally arranged and rectangularly arranged posts are both studied. For the systems with hexagonally arranged posts, the morphologies with bending alignments are most seen. We find the different kinds of patterns, which can be directly observed in experiments, are substantially induced by the pattern of the bottom layer. In the simulations with template modified with rectangularly arranged posts, by finely adjusting the distances between neighboring posts on both *x* and *y* directions, mesh-shaped structures with different angles between the bottom and the sub-bottom layers can be obtained. These results shed light on better designing lithographically patterned materials in the scale of 10 nm via the directed self-assembly of BCPs by templating.

1 Introduction

Self-assembly of block copolymers (BCPs) on patterned substrate had been a hot topic in the recent decade, because its microphase separation behavior can generate arrays of microdomains at the scale of 10 nm[1,2], which are used as lithographic patterns in the manufacture of devices, e.g., circuit boards, nanocrystal flash memories, nanowire transistors, gas sensors, bit-patterned magnetic recording medias, etc[3–10]. For example, during the manufacture of integrated circuits, the difficulty in process is to scale the photolithographic techniques used in fabrication of complementary metal oxide semiconductor transistors to below 30 nm. Applying the BCP lithography not only makes the feature sizes below 30 nm, but also dictates this size flexibly by tuning the BCP's molecular weight. Because the post arrays on the template require much less time to write than the entire layout, the templated self-assembly technique of BCP lithography is acknowledged much advantageous. The electron-beam lithography technique is often used to define these templates[2,11–15]. By functionalizing the posts with majority (minority)-block homopolymer brush, the posts can turn to be attractive (repulsive) to the majority-block matrix and repulsive (attractive) to the minority-block cylindrical microdomains. At present, the challenge in template design addresses on finding the critical template features to drive the BCPs to form a desired final pattern with as less complexity as possible. Based on that, by taking into account of the commensurability between the post period and the equilibrium BCP period, the self-assembled structures can be analyzed[16].

Intuitively, the self-assembled morphology of BCP is mastered by different factors, e.g., the arrangement style of the posts (e.g., square or hexagonal arrays), distance between neighboring posts and the geometric features of the posts (e.g, cylindrical or quadrangular posts), etc. However, it is plausible that the reality is more complex than we can imagine. In Ref.[11] the authors stressed that the self-assembly was insensitive to the post size, based on the obtained different morphologies of BCP microdomains, e.g., jogs, zig-zags and cross-points. They also demonstrated two specific and distinct techniques for the formation of such complex structures. In the first technique, for determining the overall in-plane direction of the cylinders, the post period should be set with an appropriate commensurate condition. For example, by varying the spacing between two neighboring posts in *x* and *y* directions, a broad range of BCP lattice orientation angles could be achieved. In their work they found the polystyrene-b-polydimethylsiloxane (PS-b-PDMS) could organize into cylinders parallel to the substrate and in-line with posts, when the PDMS-coated posts were set as rectangular arrays (notably the posts and template were minority favored). Besides, the cylinders could be directed by changing the post lattice geome-

[a] Institute of Theoretical Chemistry, State Key Laboratory of Supramolecular Structure and Materials, Jilin University, Changchun 130021, China
[b] Eduard-Zintl-Institut für Anorganische und Physikalische Chemie, Technische Universität, Darmstadt 64287, Deutschland
[c] School of Computer Science and Technology, Changchun University of Science and Technology, Changchun, 130022, China
[a] Institute of Theoretical Chemistry, Jilin University, Changchun 130021, China

† Electronic Supplementary Information (ESI) available: [several discussions indicated in the paper are inclosed in the Supplementary Information]. See DOI: 10.1039/b000000x/

‡ hongliu@jlu.edu.cn.

try into different turns. In the second technique, as presented in their paper, it was effective to induce the complex structures by making some posts at key positions into the shape of dashes and adding guiding posts. A recent work by Zhang et al's.[17] supplied another strategy of this route by employing the anisotropic posts, in which they used elliptical nanoposts to generate long-range ordered cylinders with single orientation. Nevertheless, different from Ref.[11]'s viewpoint, in other groups' works, the post diameter and height were proved to also influence the self-assembly pattern. Ref.[14] showed that when the post diameter was larger than 12nm, the area fraction of the BCP cylinders oriented along the commensurate orientation decreased and the cylinders broke into shorter segments. The authors also indicated the optimum post height and diameter to obtain effective templating. They demonstrated that the diameter and height of posts were major factors determining the effectiveness of the templating, by influencing the interaction between BCP cylinders and posts. Another evidence is based on the simulation by Liu and the co-workers[18], in which they used Monte-Carlo method to simulate the microphase separation of BCPs dispersed in nanorod arrays grafted on the plate. By varying the inducing height of nanorod and its grafting density in the bottom, they observed different morphologies at top and bottom of the film in the nanorod arrays. It should be noted that, recently Cao et al.[19] used self-consistent field theory model to demonstrate how the critical factors such as the height, radius and periodicities of posts affected the arrangement of cylindrical polymer structure. And notably, they exhibited that the formation of interconnections between the top and bottom layers was susceptible to the template thickness. This work showed an abundant and significant mechanical study of directed self-assembly of BCP in both qualitative and quantitative aspect.

Although different validations and predictions were made to well fit the corresponding experiments, we still need to notify the difference between the simulation and the experimental conditions. As indicated by Alexander-Katz and his co-workers[20], there are major differences between these two conditions. The simulations assume period boundary conditions of post lattices which is actually finite area without apparent boundaries between posts and cylinder structures. Besides, when the kinetically trapped structures form in experiments, the exact correspondence between experiment and simulation may departure. Despite this, the simulations give good qualitative agreement and useful predictions to experiment. Therefore, it is reasonable to extend more studies on this issue with different generic simulations, so that the complete prediction of self-assembly morphologies based on templating in experiments is possible.

In this paper, we use the particle-based dissipative particle dynamics (DPD) simulation method to study this system. This method is objective to describe such self-assembly process, and besides different technical problems are easy and flexible to be handled in simulations. Two sets of systems, which are scarcely concerned and reported by previous literatures, will be covered in this study. The first study focuses on the self-assembly of BCPs on the template with hexagonally arranged posts, in which the gap between neighboring posts can be adjusted by one parameter. The other study is based on the commonly concerned rectangularly arranged posts, while we make them as minority-unfavored. We regulate the interaction parameter between the uniform posts and different polymer components to represent the selectivity of coated template. The bottom and sub-bottom layers will be especially focused, since they are crucial for discovering the true law of the dependence of the morphology on the confinement from posts. We find in systems with hexagonally arranged posts, the minority is hard to find an obvious direction contributed by the confinement of posts, which should be account for the geometric feature of hexagonal arrangement. With the study on the system with rectangularly arranged posts, we find by continuously adjusting the distance between neighboring posts along x and y directions, a variety of mesh-shaped structures with different angles between layers can be obtained. These angles may be dependent on the correlation of the diagonal size between posts and the intrinsic period of the cylinders of BCPs. This work should help to pave the way for designing lithographically patterned materials in the scale of 10 nm.

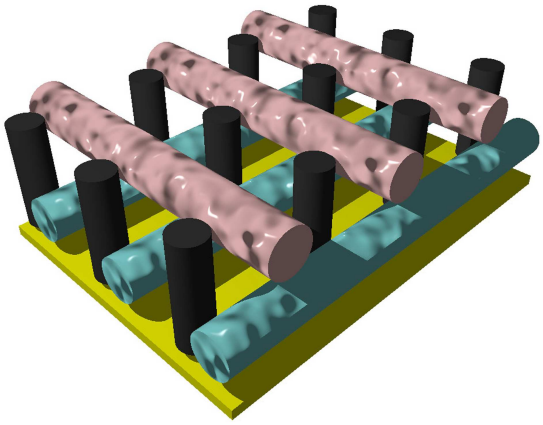

Fig. 1 Schematic illustration of the model of BCP self-assembly on the template modified with arranged posts. The yellow plate represents the template surface. The black pillars standing perpendicular to the template are the regularly arranged posts. The cyan cylinders lying between the posts represent the minority cylindrical microdomains of the bottom layer by BCP self-assembly. For comparison, the minority microdomains of the sub-bottom layer are represented as pink cylinders. The majority of BCP is not shown for clarity.

2 Model and simulation details

In DPD method, the time evolution of the interacting particles is governed by Newton's equations of motion[21]. Interparticle interactions are characterized by pairwise conservative, dissipative, and random forces acting on a particle i by a particle j. They are

given by:

$$\begin{aligned} \mathbf{F}_{ij}^{C} &= -\alpha_{ij}\omega^{C}\left(r_{ij}\right)\mathbf{e}_{ij}, \\ \mathbf{F}_{ij}^{D} &= -\gamma\omega^{D}\left(r_{ij}\right)\left(\mathbf{v}_{ij}\cdot\mathbf{e}_{ij}\right)\mathbf{e}_{ij}, \\ \mathbf{F}_{ij}^{R} &= \sigma\omega^{R}\left(r_{ij}\right)\xi_{ij}\Delta t^{-1/2}\mathbf{e}_{ij}, \end{aligned} \quad (1)$$

where $\mathbf{r}_{ij}=\mathbf{r}_i-\mathbf{r}_j$, $r_{ij}=|\mathbf{r}_{ij}|$, $\mathbf{e}_{ij}=\mathbf{r}_{ij}/r_{ij}$, and $\mathbf{v}_{ij}=\mathbf{v}_i-\mathbf{v}_j$. ξ_{ij} is a random number with zero mean and unit variance. α_{ij} is the repulsion strength, which takes the value of 25 for the particles of same kind in our simulations[21]. The parameter α_{ij} between differing species is often set as larger than 25, representing the degree of compatibility between them. $\omega^{C}\left(r_{ij}\right)=1-r_{ij}$ for $r_{ij}<1$ and $\omega^{C}\left(r_{ij}\right)=0$ for $r_{ij}\geq 1$ such that the conservative forces are soft and repulsive. The weight functions $\omega^{D}\left(r_{ij}\right)$ and $\omega^{R}\left(r_{ij}\right)$ of the dissipative and random forces couple together to form a thermostat. Español and Warren[22] showed the correct relations between the two functions,

$$\begin{aligned} \omega^{D}(r) &= \left[\omega^{R}(r)\right]^{2}, \\ \sigma^{2} &= 2\gamma k_{B}T. \end{aligned} \quad (2)$$

We take a simple choice of $\omega^{D}(r)$ due to Groot and Warren[21],

$$\omega^{D}(r)=\left[\omega^{R}(r)\right]^{2}=\begin{cases}(1-r)^{2} & (r<1)\\ 0 & (r\geq 1)\end{cases}. \quad (3)$$

It should be noted that the choice of $\omega\left(r_{ij}\right)$ is not unique and is the simplest form adopted here because of its common usage in roughly all published works.

GW-VV algorithm[21,23] is used for numerical integration,

$$\begin{aligned} \mathbf{r}_i(t+\Delta t) &= \mathbf{r}_i(t)+\Delta t\mathbf{v}_i(t)+1/2\,(\Delta t)^{2}\mathbf{f}_i(t), \\ \widetilde{\mathbf{v}}_i(t+\Delta t) &= \mathbf{v}_i(t)+\lambda\Delta t\mathbf{f}_i(t), \\ \mathbf{f}_i(t+\Delta t) &= \mathbf{f}_i\left(\mathbf{r}(t+\Delta t),\widetilde{\mathbf{v}}(t+\Delta t)\right), \\ \mathbf{v}_i(t+\Delta t) &= \mathbf{v}_i(t)+1/2\Delta t\left(\mathbf{f}_i(t)+\mathbf{f}_i(t+\Delta t)\right). \end{aligned} \quad (4)$$

We choose $\lambda=0.65$ and $\Delta t=0.05$ here according to Ref.[23].

In our simulations, the radius of interaction, the particle mass, and the temperature are set to be units, i.e. $r_c=m=kT=1$. The particle density ρ is kept equal to 3. Polymers are constructed by connecting the neighboring beads together via the harmonic springs $\mathbf{F}_i^{S}=\sum_j C\mathbf{r}_{ij}$. We choose the spring constant $C=10$ according to Ref.[23].

The bulky BCP in the simulation is chosen as a mixture of A_3B_7 with the volume fraction 70% and A_2B_8 with the volume fraction 30%, so that the 27% minority fraction is exactly at the typical region of cylindrical structure in the BCP phase separation diagram[24,25]. The interaction parameter between minority and majority is set as $\alpha_{AB}=45$ according to the Flory-Huggins parameter $\chi N=58$ introduced in Ref.[24]. Because α_{AB} is set as a constant during this work, we use $\triangle\alpha=\alpha_{PB}-\alpha_{PA}$ to represent the post selectivity of BCPs, in which α_{PA} represents the interaction between the post and minority while α_{PB} represents the interaction between the post and majority. $\triangle\alpha>0$ implies posts favor the minority A otherwise favor the majority B[26]. The repulsion strengths between the template surface and BCP components are set as $\alpha_{TA}=45$ and $\alpha_{TB}=25$ to avoid the minority paving on the template which may influence the phase separation. The model is constructed by two planar templates with the posts regularly arranged on the bottom one, and the bulky BCP chains filled in the unoccupied space between the two templates. The periodic boundary conditions are applied in both x and y directions. The template and the posts are constructed by extracting the positions of a group of particles with the corresponding geometric shape from liquid amorphous configuration of bulky BCP and setting them as frozen, so that there are less density fluctuations of free particles at the boundaries of the frozen template or posts with the bulk. Furthermore, to keep the template impenetrable in DPD simulations, a bounce-back reflection condition is imposed on the template surface so that the free particles can move back correctly into the fluid[27]. It should be noted that, we extend this condition on a geometric point of view as well, i.e., when the free particles hit the the side surface of the post, the top face of the post, or even at the corner between the base of post and the template, it can bounce back according to the correct geometric reflection trajectory. All simulations are performed using GALAMOST[28] package on Nvidia GTX780 cards.

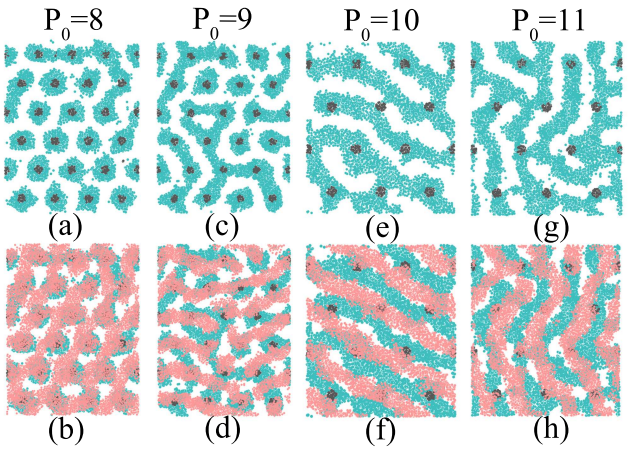

Fig. 2 Top view of morphologies by templated self-assembly of BCPs with different distances of hexagonally arranged posts P_0. The posts are set to favor the minority but unfavor the majority ($\triangle\alpha=20$). The height of post is set as $h=7$ and the radius $r=1$. The black dots represent the positions and sizes of posts. The cyan part represents the morphology formed by the bottom layer of minority near the template, while the pink part represents the sub-bottom layer of minority. Thus the top row (a, c, e and g) is the morphology of only the bottom layer, while the down row (b, d, f and h) is a overlapped morphology of both the bottom layer and sub-bottom layer. The majority of BCP is not shown for clarity.

Before the simulations, with a test simulation of such bulky BCPs, we have obtained that the equilibrium width of the hexagonally arranged cylindrical microdomains is around $L_0=7$ of reduced unit, while the diameter of them is around $R_0=3.5$. Based on that, the height between the top and bottom template is set as 35.5 so that around 6 layers of hexagonally arranged cylin-

ders can be expected to be occupied (detailed discussion about the choice of this height value can be found in the Supplementary Information). With this choice of height, the top template can be considered to have no influence on the bottom and sub-bottom layer of cylindrical microdomains affected by the posts. The box sizes at x and y directions are set variable depending on the distance between neighboring posts, so that the posts can be considered periodically regularly arranged with the periodic boundary conditions in both directions. Fig. 1 shows the schematic illustration of the self-assembly of BCPs on the template modified with arranged posts.

The simulations are conducted in canonical NVT ensemble. After generating the initial configuration, 2.5×10^5 steps integrations are carried out to ensure that the systems are well relaxed. For obtaining the equilibrated morphologies of self-assembly, basically another period of at least 1×10^6 simulations after relaxation are conducted for all systems. It should be noted that, for those systems which are suspectable in metastable state, a process including loops of anneals are additionally conducted. With the aid of multi-cycle annealing technique, it turns easier to achieve ordered structure and to escape from the metastable states. We start from an initial temperature 1.0 of reduced unit, i.e., $T^* = 1.0kT/\varepsilon$, then increase the temperature with the interval of 0.3 for keeping a period of 5×10^5 time steps simulation each time, until it reaches to the target temperature of 2.5. Later a completely same backward route of cooling down process is conducted until the temperature gets to 1.0 again. Such an annealing cycle is conducted for three times for each sample. As our experiences, the annealing process is crucial to eliminate the local defects and further to improve the stable ordered structures of BCP assembly.

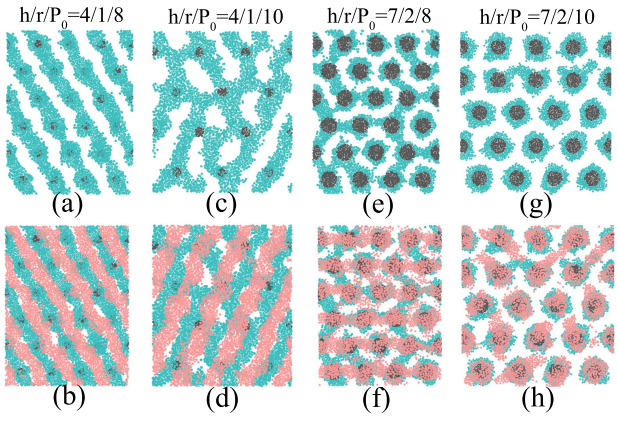

Fig. 3 Top view of morphologies by templated self-assembly of BCPs with different sizes of hexagonally arranged posts (different post height h and post radius r) as well as with different gaps between neighboring posts P_0. The representations are the same as that in Fig. 2. The denotation "$h/r/P_0$" is followed with the respective values of h, r and P_0 for the space saving. The majority of BCP is not shown for clarity.

3 Results

For most of relevant studies about self-assembly of BCPs by templating, in practice, squarely or rectangularly arranged arrays of posts are most seen, because the square arrays are more compatible with semiconductor integrated circuit design standards. As Ref.[29] indicated, in practice the chemical patterns are written on a rectangular lattice because the e-beam moves in an x-y grid with discrete steps along the x and y axis. With different application background, other important arrays are with great significance as well, e.g., the hexagonal arrays of posts[2]. Compared with rectangularly arranged posts, BCP self-assembly on template with hexagonally arranged posts has scarcely reported. In previous reports, Ross and co-workers had demonstrated that in specific conditions, well-defined hexagonal arrays of posts could generate well-ordered hexagonal arrays of spheres[2]. In our simulations a general phenomenon is that deformed cylindrical morphologies can be obtained. Templating hexagonal arrays of posts is another strategy of routing of nanoscale cylindrical features using self-assembly of BCP.

3.1 Hexagonally arranged posts

In this section, the posts are set as minority-favored to reproduce the experimental conditions[14,16], i.e., $\triangle\alpha = 20$ (the substrate is set as minority-unfavored and the corresponding discussions can be found in Supplementary Information). The distance between neighboring posts (post centers) is defined as P_0. In this set of simulations, the height of posts is set as $h = 7$ and the radius of posts is set as $r = 1$. As shown in Fig. 2, by adjusting the value of P_0 from 8 to 11, different but regular morphologies of BCPs can be observed. In Fig. 2 a&b with $P_0 = 8$ (comparable to the equilibrium width of cylindrical microdomains L_0), from the bottom layer it is clear that each post is surrounded by the separated domains of minority and scarcely has connection to neighbors. The sub-bottom layer of minority while can form connected irregular dotted domains. As compared to the results in square arrays of posts (e.g.Ref.[14]), it may be ascribed to that hexagonally arranged posts show relatively obscure channels for the BCPs to direct the cylindrical domains, which accounts for that the distances between any two neighboring posts are completely the same. As a consequence, it is hard for the minority to obtain a determined direction to lay its cylindrical domain. With almost uniform attractions from the posts around the minority, it is decomposed into different small microdomains of the same size to wrap each post. Based on this stable morphology of the bottom layer, the sub-bottom layer is induced to form similar dotted domains but with overall much more connections between neighboring domains. A similar morphology had been reported in Bita et al.'s experiments[2] in which they focused on the templated self-assembly of PS-b-PDMS BCPs on substrate modified with hexagonally arranged posts. This structure is potentially applicable for manufacturing a parallel circuit which has a plurality of connection points on bottom surface. By increasing the distance to $P_0 = 9$, the separated cylinders of bottom minorities which surround the posts start to connect with neighboring ones. However the short segments still have no obvious alignment from

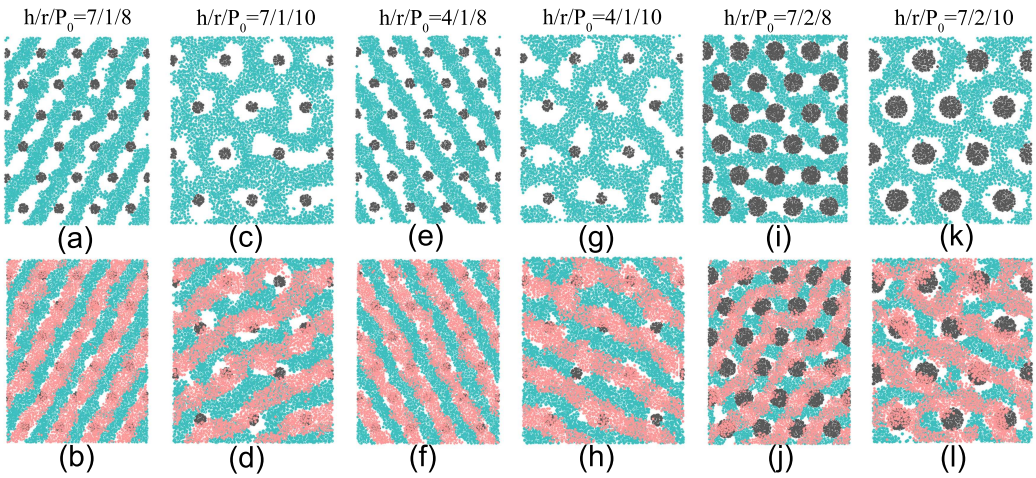

Fig. 4 Top view of morphologies by templated self-assembly of BCPs with different sizes of hexagonally arranged posts (different post height h and post radius r) as well as with different gaps between neighboring posts P_0. The posts are set to favor the majority but unfavor the minority. The representations are the same as that in Fig. 2. The denotation "$h/r/P_0$" is followed with the respective values of h, r and P_0 for the space saving. The majority of BCP is not shown for clarity.

templating. This result is counterintuitive, because the increased gaps between posts from Fig. 2a to Fig. 2c however lead to the general linkage of neighboring microdomains which are almost completely separated in the former. $P_0 = 9$ is apparently larger than the equilibrium period of cylindrical BCP L_0, thus the enlarged gaps provide enough space for the cylinders to completely align between the posts. Therefore, the minority microdomains tend to link with their neighbors to form short linear segments to lower the energy. As an induced result of bottom layer, this explanation still applies to the sub-bottom layer which also forms short cylindrical segments parallel to the template, as shown in Fig. 2d. With a further increase of P_0 to 10, we find the confinement from the placement of posts to BCP self-assembly becomes even weaker, thus the bottom minority can randomly find a channel for alignment and form fuzzy cylindrical morphology with bulges, see Fig. 2e. Accounting for induced by the bottom layer, the sub-bottom minority forms obvious striped alignment along the commensurate orientation while vertically staggers with the bottom minority. With further increase to $P_0 = 11$ which is much larger than L_0, we find basically cylindrical morphology of bottom layer but with obvious turns near posts. As compared, the sub-bottom layer shows even obvious regular alignments with similar turns, as shown in Fig. 2 g&h. This set can be considered as a recovered morphology of $P_0 = 10$, since the enlarged gaps between posts have less confinement to the self-assembly of BCPs. The morphologies with even larger P_0 should be reasonably similar. One may doubt that the morphology with turns should be attributed to the metastable state in simulation, while interestingly we have not found any improvement of the morphologies after several independent annealing processes. In sum, with an increase of P_0 from around the BCP cylinder's bulky period to larger, the confining effect of post to the morphology is reduced. As a result, the bottom layer of minority tends to form the morphology close to its bulky cylinders. The morphology of bottom layer further induces the sub-bottom layer to form striped alignment or with turns.

In Fig. 3, we can also find the comparison of morphologies with different P_0 values. In Fig. 3 a&b and c&d, it shows the influence of P_0 on the BCP morphologies with shorter posts of height $h = 4$. It is clear for shorter posts, P_0 can only affect the morphology of the bottom minority instead of both the two layers. From $P_0 = 8$ to $P_0 = 10$, the bottom minority changes from stripped cylinders parallel to the template to interconnected morphology. Another comparison is seen between Fig. 3 e&f and g&h, which are with the same large post with radius $r = 2$. It is apparent that with smaller gap $P_0 = 8$, the bottom minority shows interconnected domains centered with the posts. While for larger gap $P_0 = 10$, it is hard for the domains to connect with each other, thus they become separated. This difference yields the dissimilarity of the morphologies of sub-bottom minority. In the system of $P_0 = 8$ the sub-bottom minority shows long parallel stripes with bulges (Fig. 3f), while with $P_0 = 10$ we find the sub-bottom minority forms separated short thick domains.

As a parallel comparison, we study the influence of the post geometric feature on the morphology of BCP self-assembly. The increase of the height and radius of post exactly causes the increase of post superficial area, which may further induce the increased fraction of minority attracted by posts. Thus with appropriate gaps between post, isolated minority dot morphologies are expected to be obtained. The comparison between Fig. 2 a&b and Fig. 3 a&b shows the influence of post height on the morphology with $P_0 = 8$ and $r = 1$. With the decrease of height of the post, we achieve the obvious alignment of cylinders parallel to the template on both the bottom layer and the sub-bottom layer in Fig. 3 a&b (it can also be observed from the three-dimensional (3D) image of this morphology in Fig. 5a). This result seems hard

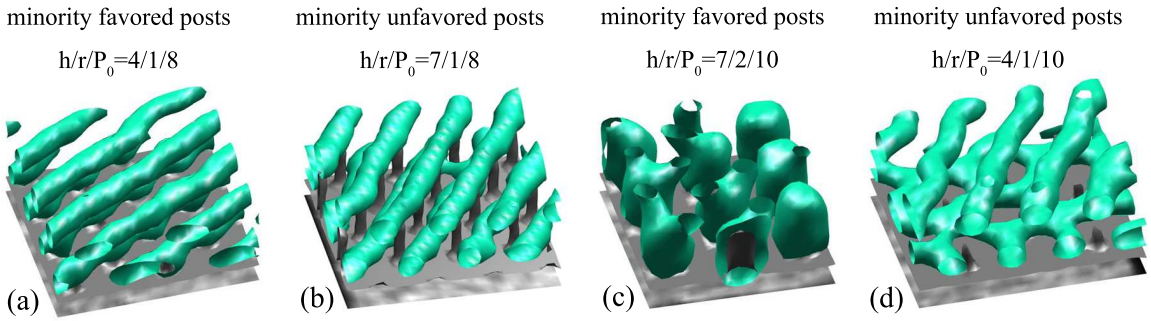

Fig. 5 3D images of typical morphologies in systems with hexagonally arranged posts.

to understand since as compared to Fig. 2a, there is no change of confinement for the bottom layer of minority by only lowering the height of post. In Fig. 3a, the short posts with $h = 4$ has no confining effect on the sub-bottom layer, therefore it naturally tends to form the striped aligned cylinders as in bulk (i.e., in Fig. 3b). When the posts are short enough so that the bottom layer can feel the disappearance of confinement from its top, there may be an effect of inverse inducement from the sub-bottom layer to the bottom. As a result, the bottom layer basically follows the contour of aligned cylindrical morphology, meanwhile has the trend to form broken individual domains because of the existence of posts, as that in Fig. 3a. Another comparison is between Fig. 2 e&f and Fig. 3 c&d that with $P_0 = 10$, $r = 1$ but with different heights of post. We find as the gap is enlarged as $P_0 = 10$, the effect of post height is decreased, i.e., no obvious difference of the morphologies between systems with $h = 4$ and $h = 7$. On the other hand, the comparison between Fig. 2 a&b and Fig. 3 e&f shows the influence of post radius on the BCP self-assembly (with the same post height $h = 7$). By the increase of post radius, the connections between minority domains are increasing. While the sub-bottom layer seems having no obvious change with r. Another comparison is between Fig. 2 e&f and Fig. 3 g&h that with $P_0 = 10$ and $h = 7$. As the post radius is increased, the space for the BCP becomes narrower, thus the bulk-like cylinders in the system of $r = 1$ is broken into small domains (it can also be observed from the 3D image of this morphology in Fig. 5c). Correspondingly, the sub-bottom layer induced by the bottom layer is also changed to separated domains, as shown in Fig. 3 g&h. It should be noted that, in Ref.[14] with squarely arranged posts, the authors also stressed that post height and diameter would affect the self-assembly. They indicated that when the post diameter are as comparable or smaller than the size of BCP cylinders, the distortion of microdomains would be minimized and when the post was very high, the template could promote the alignment of the cylinders along the arrays. In the present study with hexagonally arranged posts, the effects of r and P_0 may be generalized to the substantial space between posts, which should be crucial on forming the confinement to the self-assembly of BCPs. Besides, the height of the post h should determine the morphologies of upper layers, which may further be induced by or inversely induce the bottom layer.

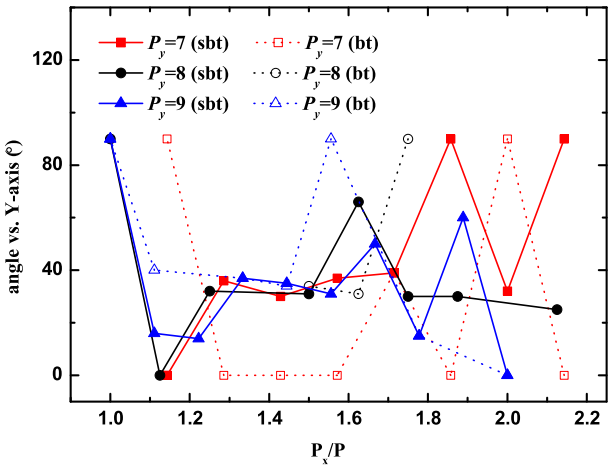

Fig. 7 Dependence of the angles between the orientation of the bottom layer versus the y-axis (denoted as "bt" with hollow symbols) and the sub-bottom layer versus the y-axis (denoted as "sbt" with solid symbols) on the value of P_x/P_y. Each symbol corresponds to a subfigure in Fig. 6. The ones with obscure bending cylinders are not shown.

As a further investigation, we study the condition when the posts favor the majority but unfavor the minority (i.e., $\triangle\alpha = -20$), as shown in Fig. 4. In this condition, the minority stays away from the post, meanwhile tends to be aligned along the commensurate orientation. We find when the distance between posts is set appropriately (e.g., with $P_0 = 8$), the minority can keep alignment perfectly, see Fig. 4 a&b and Fig. 4 e&f (3D image of morphology in Fig. 4 a&b can also be found in Fig. 5b). When the gap becomes larger (e.g., with $P_0 = 10$), interconnected network morphology of the bottom layer is obtained, see Fig. 4

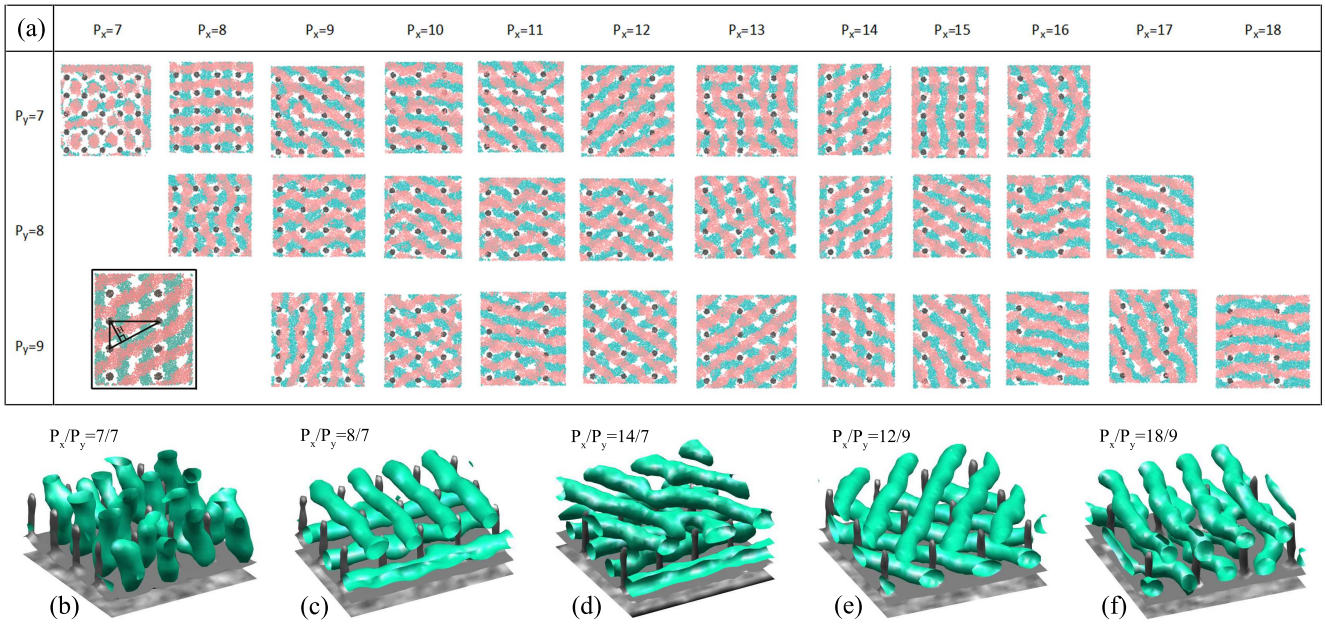

Fig. 6 (a) Top view of morphologies by templated self-assembly of BCPs with different distances of rectangularly arranged posts P_x and P_y. The posts are set to favor the majority but unfavor the minority. The post height is set as $h = 7$ while its radius is set as $r = 1$. The representations are the same as that in Fig. 2. Each picture shows the overlapped morphology of both the bottom layer and sub-bottom layer. The majority of BCP is not shown for clarity. The inset on the left bottom schematically shows the period of posts in diagonal direction which is defined as H in this paper; (b $\sim$ f): 3D images of typical morphologies in systems with rectangularly arranged posts. The post height and radius are the same as that in (a).

c&d and Fig. 4 g&h (see also Fig. 5d as the 3D image of morphology in Fig. 4 g&h). On the other hand, increasing r implies decreasing the gap between posts, therefore the orientation of alignment is blocked and the straight cylinders become obviously bending, as shown in Fig. 4 i&j. When P_0 and r are increased simultaneously, the minority becomes interconnected as well, see Fig. 4 k&l. As compared it with Fig. 4 a&b, although the absolute gap between neighboring posts does not change, the placement of large posts still affect the BCP morphology seriously. It is clear that sub-bottom layer generally stays straight alignment conformation, but the size is dependent on the bottom layer. When the bottom layer is with aligned conformation, the sub-bottom layer shows commensurate orientation but vertically staggers with the former, see Fig. 4b and Fig. 4f. When the bottom layer is with interconnected morphology, the sub-bottom layer tends to become thicker and with turns, see Fig. 4d and Fig. 4h. Besides, in this set we have not found the influence of post height on the BCP self-assembly, with the comparison between Fig. 4 a&b and Fig. 4 e&f, as well as between Fig. 4 c&d and Fig. 4 g&h. It implies that when the minority tends to keep away from its unfavorable posts, the influence of post height becomes weak. It is concluded that with hexagonally arranged posts templating, because of its geometric feature that all of the gaps between neighboring posts are identical, the BCPs are difficult to feel an obvious directed confinement during its self-assembly, therefore it is not easy to obtain perfect aligned morphology. Commonly, the alignments with turns or interconnected morphologies are more often to be observed.

3.2 Rectangularly arranged minority-unfavored posts

The self-assembly of BCPs by templating with rectangularly arranged posts had been studied previously[29–31]. Here we make a brief study on the minority-unfavored posts which are less reported in experiments[16,32]. It had been shown that by using an array of minority-unfavored posts, it was possible to locally control the morphology of BCP, to achieve several morphologies simultaneously on a single substrate, and to create patterns with square or rectangular symmetry[32]. The interaction parameter is set as $\triangle\alpha = -20$ in this study. The results are shown in Fig. 6 and Fig. 8, with post radius $r = 1$ and $r = 2$, respectively. P_x and P_y represent the distance between neighboring posts (post centers) in x and y direction, respectively. Similar to the system with hexagonally arranged posts, the side lengths of simulation box in x and y directions are set integer multiples of P_x and P_y. P_y is finely adjusted from $7 \sim 9$ and P_x changes from equivalent of P_y to more than $2P_y$. In the two sets of simulations, the aligned morphologies are basically generated.

Fig. 6a shows that with the post radius $r = 1$ most systems are with aligned cylindrical morphologies, except for the separated domain structure when $P_x = P_y = 7$. With $P_x = 7$ and $P_y = 7$, the substantial gaps between neighboring posts are equal to 5, obviously smaller than L_0, where the minority cylinders are eventually broken into short segments or small domains. In Fig. 6 b$\sim$f sev-

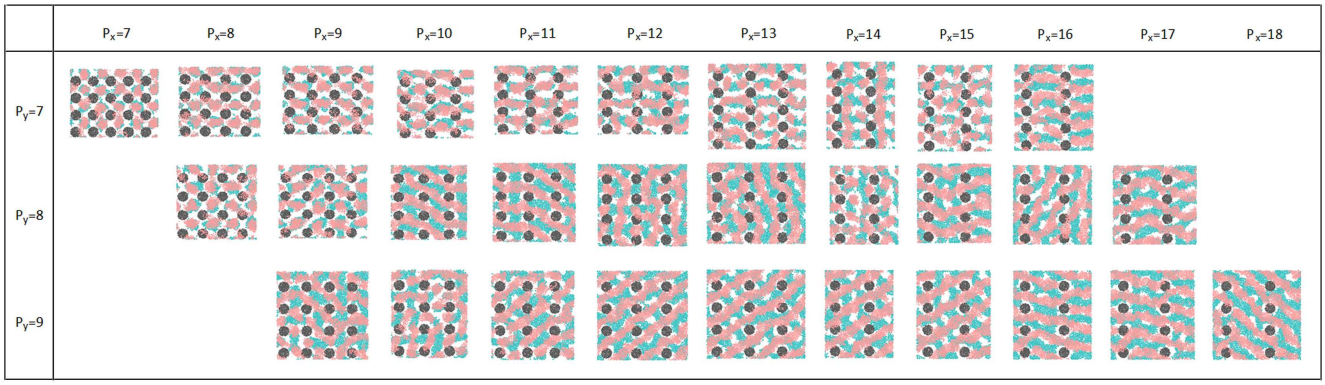

Fig. 8 Top view of morphologies by templated self-assembly of BCPs with different distances of rectangularly arranged posts P_x and P_y. The posts are set to favor the majority but unfavor the minority. The post height is set as $h = 7$ while its radius is set as $r = 2$. The representations are the same as that in Fig. 2. Each picture shows the overlapped morphology of both the bottom layer and sub-bottom layer. The majority of BCP is not shown for clarity.

eral 3D images of typical morphologies obtained in Fig. 6a with rectangularly arranged posts are presented. It is clear that by adjusting the values of P_x and P_y, the morphologies in which the cylinders of bottom and sub-bottom layers crossing into perpendicular mesh-shaped or angled mesh-shaped structures can be obtained. A part of the morphologies well fit those occurred in previous studies. For example, the three subfigures in Fig. 6a ($P_y = 7$ and $P_x = 8$; $P_y = 7$ and $P_x = 14$; $P_y = 9$ and $P_x = 12$) basically agree with the observations of Cao et al. (corresponding to the three subfigures of Fig.3 in Ref.[19] respectively, in which $R_g \sim 10nm$ of their work). The subfigure of $P_y = 7$ and $P_x = 8$ also agrees with the system labeled as solid square in Fig.4b of Ref.[19] and system of Fig.5g of Ref.[33], while the subfigures of $P_y = 7$ and $P_x = 14$ and 15 agree with the system labeled as solid circle in Fig.4b of Ref.[19], both on morphologies and parameters. Besides, the special structures such as the "Y-shaped" junctions in Fig.5k and i of Ref.[33] can be found in the morphology of subfigure with $P_y = 7$ and $P_x = 7$ of Fig. 6a. Although some of the cylinders are bending, we still can basically plot out the orientations of the layers in each morphology. In Fig. 7 we plot the dependence of the angles between the orientations of the bottom and sub-bottom layers versus the y-axis on the value of P_x/P_y. When each hollow symbol gets closer to its solid counterpart, it indicates that the bottom layer and the sub-bottom layer are commensurately directed. When the two symbols denote obviously different values, it indicates the two layers tend to form perpendicular mesh-shaped structure. As shown in Fig. 7, for $P_y = 7$ the orientation of the bottom layer is commonly along the y-axis. There are several systems with perpendicular mesh-shaped structure for $P_y = 7$, i.e., $P_x/P_y = 1.14$, 1.85 and 2.14. For $P_y = 8$ and 9, structures with commensurate parallel cylinders of both layers are more common. Angled mesh-shaped structures can also be found for $P_y = 8$ and 9. In the region of $P_x/P_y = 1.2 \sim 1.6$, a generally parallel or small angle mesh-shaped cylindrical morphology is obtained. In the region with $P_x/P_y > 1.6$, we basically find large discrepancy of orientations between the two layers. These analyses may support the viewpoint that mesh-shaped structures occur when the post period in the x or diagonal direction is equal to the BCP period L_0, while the period in the y direction was comparable or slightly less than an integer multiple of the BCP period[16]. Because when $P_x/P_y \approx 1.6$, the diagonal direction is around $1.89P_y$, which is around double of L_0. On the other hand, with a closer observation of the systems in Fig. 8, it is easy to find typically regular morphologies, while most alignments are greatly biased by the placements of large sized posts with $r = 2$. With a parallel comparison between Fig. 6 and Fig. 8, we find the cylinders consisting of minority with post radius $r = 1$ is easier to form consequent cylinder morphologies than that of $r = 2$, and the separated domain structures with $r = 2$ are correspondingly more common than those in $r = 1$, since the ordered posts with larger sizes are more likely to break the directions, as well as the period of cylinders in BCP assembly. It should be noted that, Cao et al.[19] had observed a transition of cylinders from the parallel to perpendicular orientations by increasing the post height in their systems with minority-unfavored rectangularly arranged posts. In Supplementary Information we provide a phase diagram of the morphologies dependent on the post height and radius, in which basically a similar transition can be observed as the increase of post height. This result partially supports Cao et al.'s conclusions.

For further investigating the dependence of the morphologies on the distances between neighboring posts, we define another parameter H which represents the periodicity of posts in another typical direction (as shown the inset of Fig. 6a), i.e., $H = P_xP_y/\sqrt{P_x^2 + P_y^2}$. Based on the morphologies in Fig. 6, there are several typical structures in which the cylinders in sub-bottom layer arrange along a diagonal direction, i.e., those with

$\{P_y = 8, P_x = 14;\ \ P_y = 8, P_x = 15;\ \ P_y = 9, P_x = 12;\ \ P_y = 9, P_x = 13;\ \ P_y = 9, P_x = 14\}$, where H equals to $\{7.2;\ 7.4;\ 7.0;\ 7.59;\ 7.05\}$ respectively, in the range of $7.0 \sim 7.6$. Obviously H is comparable to the period of bulky cylinders L_0 which is approximately equivalent to 7. If H is smaller than 7, the cylinders on both the two layers tend to bend, like $P_y = 8, P_x = 12$ and $P_y = 8, P_x = 13$. If H is larger than L_0, the cylinders on both two layers tend to bend as well, like $P_y = 8, P_x = 16$ and $P_y = 8, P_x = 17$. As a further classification, the typical S-shaped cylinders emerge at $P_y = 8$, and $P_x = 8 \sim 12$ respectively. In these systems the cylinders cannot array straightly since H does not meet the period L_0. As compared, this rule works as well in the system with larger post size, as shown in Fig. 8. The structures in which cylinders in sub-bottom layer arrange along diagonal direction include those with $P_y = 9$ and $P_x = 12 \sim 15$, where H equals to $7.0 \sim 7.8$. This result agrees with that when the parameter H meets the period of bulky cylinders, alignment morphologies along diagonal directions are possibly obtained. Interestingly, these morphologies seem to be less influenced by the ordered large posts like other systems in Fig. 8 which are driven to bend or even broken microdomains. This kind of perfect straight morphologies may imply that the alignments along the diagonal directions are the optimized most stable states during the templated BCP self-assembly.

4 Conclusions

In this paper, the DPD simulations are employed to study the self-assembly of BCPs on the template modified with ordered posts. The templates with hexagonally arranged and rectangularly arranged posts are both studied. For the systems with hexagonally arranged posts, we find the morphologies with bending alignments are most seen. Accounting for the feature of hexagonal arrays, the distances between any two neighboring posts are completely the same, therefore it is hard for the minority cylinders of BCP to find out a directed channel. Besides, we find the different kinds of patterns, which can be directly observed in experiments, are substantially induced by the pattern of the bottom layer. Understanding the formation of the bottom layer morphology should be helpful to predict the structures in experiments. In the simulations with template modified with rectangularly arranged posts, we find by finely adjusting the distances between neighboring posts on both x and y directions, mesh-shaped structures with different angles between the bottom and the sub-bottom layers can be obtained. We also find when the typical H parameter meets the period of bulky cylinders, alignment morphologies along diagonal directions are possibly obtained. This study helps to pave the way on better control and design of lithographically patterned materials in the scale of 10 nm via the directed self-assembly of BCPs by templating.

5 Acknowledgment

This work is supported by the National Science Foundation of China (21474042,51403022, 51273007). We also thank the supports from Jilin Province Science and Technology Development Plan (20140101096JC) and Jilin Industrial Technology Research and Development Projects, China (JF2012C022-4). H. L. gratefully acknowledges the funding support provided by the Alexander von Humboldt Foundation.

References

1 S. O. Kim, H. H. Solak, M. P. Stoykovich, N. J. Ferrier, J. J. de Pablo and P. F. Nealey, *Nature*, 2003, **424**, 411–414.
2 I. Bita, J. K. W. Yang, Y. S. Jung, C. A. Ross, E. L. Thomas and K. K. Berggren, *Science*, 2008, **321**, 939–943.
3 M. P. Stoykovich, H. Kang, K. C. Daoulas, G. Liu, C.-C. Liu, J. J. de Pablo, M. Müller and P. F. Nealey, *ACS nano*, 2007, **1**, 168–175.
4 D. J. Milliron, S. Raoux, R. M. Shelby and J. Jordan-Sweet, *Nat. Mater.*, 2007, **6**, 352–356.
5 J. Y. Cheng, W. Jung and C. A. Ross, *Phys. Rev. B*, 2004, **70**, year.
6 C. T. Black, *Appl. Phys. Lett.*, 2005, **87**, year.
7 T. Thurn-Albrecht, J. Schotter, G. A. Kästle, N. Emley, T. Shibauchi, L. Krusin-Elbaum, K. Guarini, C. T. Black, M. T. Tuominen and T. P. Russell, *Science*, 2000, **290**, 2126–2129.
8 Y. S. Jung, W. Jung, H. L. Tuller and C. A. Ross, *Nano Lett.*, 2008, **8**, 3776–3780.
9 I. I. Perepichka, X. Chen and C. G. Bazuin, *Sci. China Chem.*, 2013, **56**, 48–55.
10 F. Zhou, Q.-H. Zhou, H.-J. Tian, C.-S. Li, Y.-D. Zhang, X.-H. Fan and Z.-H. Shen, *Chinese J. Polym. Sci.*, 2015, **33**, 709–720.
11 J. K. W. Yang, Y. S. Jung, J.-B. Chang, R. A. Mickiewicz, A. Alexander-Katz, C. A. Ross and K. K. Berggren, *Nat. Nanotechnol.*, 2010, **5**, 256–260.
12 J. G. Son, J.-B. Chang, K. K. Berggren and C. A. Ross, *Nano Lett.*, 2011, **11**, 5079–5084.
13 C. G. Hardy and C. Tang, *J. Polym. Sci. Pol. Phys.*, 2013, **51**, 2–15.
14 J.-B. Chang, J. G. Son, A. F. Hannon, A. Alexander-Katz, C. A. Ross and K. B. Karl, *ACS nano*, 2012, **6**, 2071–2077.
15 J. Feng, K. A. Cavicchi and H. Heinz, *Acs Nano*, 2011, **5**, 9413–9420.
16 A. T. K. Ghariehali, K. W. Gotrik, A. F. Hannon, A. Alexander-Katz, C. A. Ross and K. K. Berggren, *Science*, 2012, **336**, 1294–1298.
17 L. Zhang, L. Wang and J. Lin, *ACS Macro Lett.*, 2014, **3**, 712–716.
18 X. Xiao, Y. Huang, J. Feng, H. Liu and Y. Hu, *Macromol. Theor. Simul.*, 2011, **20**, 124–132.
19 X. Cao, L. Zhang, J. Gu, L. Wang and J. Lin, *Polymer*, 2015, **72**, 10–20.
20 A. T. K. Ghariehali, A. F. Hannon, K. W. Gotrik, A. Alexander-Katz, C. A. Ross and K. K. Berggren, *Adv. Mater.*, 2012, **24**, 4249–4254.
21 P. B. Groot, R. D.; Warren, *J. Chem. Phys.*, 1997, **107**, 4423–4435.
22 P. E. ol and P. Warren, *Europhys. Lett.*, 1995, **30**, 191–196.
23 R. D. Groot and T. J. Madden, *J. Chem. Phys.*, 1998, **108**, 8713–8724.
24 Y. Li, H.-J. Qian, Z.-Y. Lu and A.-C. Shi, *Polymer*, 2013, **54**,

6253–6260.
25 M. W. Matsen and F. S. Bates, *J. Chem. Phys.*, 1997, **106**, 2436–2448.
26 H. Djohari and E. E. Dormidontova, *Biomacromolecules*, 2009, **10**, 3089–3097.
27 I. V. Pivkin and G. E. Karniadakis, *J. Comput. Phys.*, 2005, **207**, 114–128.
28 Y.-L. Zhu, H. Liu, Z.-W. Li, H.-J. Qian, G. Milano and Z.-Y. Lu, *J. Comput. Chem.*, 2013, **34**, 2197–2211.
29 R. Ruiz, H. Kang, F. A. Detcheverry, E. Dobisz, D. S. Kercher, T. R. Albrecht, J. J. de Pablo and P. F. Nealey, *Science*, 2008, **321**, 936–939.
30 S.-M. Park, G. S. W. Craig, Y.-H. La, H. H. Solak and P. F. Nealey, *Macromolecules*, 2007, **40**, 5084–5094.
31 J.-B. Chang, H. K. Choi, A. F. Hannon, A. Alexander-Katz, C. A. Ross and K. K. Berggren, *Nat. Commun.*, 2014, **5**, 3305.
32 A. T. K. Ghariehali, A. F. Hannon, K. W. Gotrik, A. Alexander-Katz, C. A. Ross and K. K. Berggren, *Adv. Mater.*, 2012, **24**, 4249–4254.
33 K. W. Gotrik, T. Lam, A. F. Hannon, W. Bai, Y. Ding, J. Winterstein, A. Alexander-Katz, J. A. Liddle and C. A. Ross, *Adv. Funct. Mater.*, 2014, **24**, 7689–7697.